Integrating DVH criteria into a column generation algorithm for VMAT treatment planning

Mehdi Mahnam, Michel Gendreau, Nadia Lahrichi, and Louis-Martin Rousseau

Canada Research Chair in Healthcare Analytics and Logistics, Department of Mathematics and Industrial Engineering, Polytechnique Montréal, Montréal, Canada

E-mail: mehdi.mahnam@polymtl.ca, michel.gendreau@polymtl.ca, nadia.lahrichi@polymtl.ca, louis-martin.rousseau@polymtl.ca

February 2019

Abstract. Volumetric-modulated arc therapy (VMAT) treatment planning is an efficient treatment technique with a high degree of flexibility in terms of dose rate, gantry speed, and aperture shapes during rotation around the patient. However, the dynamic nature of VMAT results in a large-scale nonconvex optimization problem. Determining the priority of the tissues and voxels to obtain clinically acceptable treatment plans poses additional challenges for VMAT optimization. The main purpose of this paper is to develop an automatic planning approach integrating dose-volume histogram (DVH) criteria in direct aperture optimization for VMAT, by adjusting the model parameters during the algorithm.

The proposed algorithm is based on column generation, an optimization technique that sequentially generates the apertures and optimizes the corresponding intensities. We take the advantage of iterative procedure in this method to modify the weight vector of the penalty function based on the DVH criteria and decrease the use of trial-and-error in the search for clinically acceptable plans.

We evaluate the efficiency of the algorithm and treatment quality using a clinical prostate case and a challenging head-and-neck case. In both cases, we generate 15 random initial weight vectors to assess the robustness of the algorithm. In the prostate case, our methodology obtained clinically acceptable plans in all instances with only a 10% increase in the computational time, while simple VMAT optimization found just three acceptable plans. To have an idea with respect to the existing software, we compared the obtained DVH to a commercial software. The quality of the diagrams of the proposed method, especially for the healthy tissues, is significantly better while the computational time is less. In the head-and-neck case, 93.3% of the clinically acceptable plans are obtained while no plan was acceptable in simple VMAT.

In sum, the results demonstrate the ability of the proposed optimization algorithm to obtain clinically acceptable plans without human intervention and also its robustness to weight parameters. Moreover, our proposed weight adjustment procedure proves to reduce the symmetry in the solution space and the time required for the post-optimization phase.

Keywords: Volumetric-modulated arc therapy, direct-aperture optimization, dose–volume criteria, column generation.

Submitted to: *Phys. Med. Biol.*

1. Introduction

Volumetric-modulated arc therapy (VMAT) is an efficient form of external radiotherapy which has been widely used during the past decade. In this technology, the beam rotates around the patient's body while the dose rate, gantry speed, and beam shape change continuously (Otto 2008). The beams are formed by a multi-leaf collimator (MLC) that has a finite number of leaf pairs, each consisting of a leading and a trailing leaf.

Several optimization techniques have been developed for the treatment planning problem in VMAT (Otto 2008, Bedford 2009, Bzdusek et al. 2009, Cao et al. 2009, Men et al. 2010, Craft et al. 2012, Peng et al. 2012, Bokrantz 2012, Papp and Unkelbach 2014). In general, we categorize these methods into two main approaches: (1) two-stage and (2) direct aperture. In the former, at the first stage, each beam is discretized into beamlets, and fluence map optimization (FMO) is used to find the optimal intensity for each beamlet. At the second stage, the ideal fluence map is converted into a sequence of deliverable arcs, typically based on unidirectional leaf motion, maximizing the similarity of the dose distribution to the FMO plan (Craft et al. 2012, Salari et al. 2012, Papp and Unkelbach 2014, Bokrantz 2012).

In the direct-aperture approach, the apertures around the patient and the corresponding intensities are optimized subject to the MLC constraints. In this approach, the column generation (CG) technique has been widely used. This algorithm sequentially generates new apertures and optimizes the corresponding intensities, ensuring to be compatible with adjacent apertures (Men et al. 2010, Peng et al. 2012, Peng et al. 2015, Renaud et al. 2017). Unkelbach et al. (2015) provide a comprehensive review of optimization techniques for VMAT treatment planning.

Recent studies have extended VMAT optimization to take the treatment times and clinical criteria into account. Nguyen et al. (2016) developed a non-greedy approach; it uses an L_2-norm fidelity term in the objective and a level set function to simultaneously optimize the fluence intensity and aperture shapes. Balvert and Craft (2017) investigated the trade-off between delivery time and fluence map matching. They optimized the leaf trajectories and dose rates for a given delivery time and obtained the complete trade-off curve for delivery time and plan quality by solving the model heuristically with a range of delivery times. Recently, Mahnam et al. (2017) have developed a CG-based heuristic for VMAT that optimizes the trade-off between delivery time and treatment quality.

One of the main technical challenges of treatment planning is to find the optimal model parameters for generating an acceptable plan within a reasonable time. In practice, the treatment planning system (TPS) technicians solve the problem several times for each patient, taking into account various model parameters, e.g., the overdose and underdose weights for target volumes and healthy organs. This manual procedure is time-consuming, especially for complex cases.

Several researchers have studied systematic techniques for the evaluation of treatment planning. The dose–volume histogram (DVH) is the most common method for evaluating the quality of the plan. It indicates the percentage of a volume that receives at least a certain dose. For example, in prostate cancer the planner may specify that "no more than 80% of the rectum is allowed to receive 30 Gy or more." Two approaches have been developed to handle DVH criteria. The first adds dose–volume constraints (DVCs) directly to the mathematical model, and the second automatically adjusts the penalty parameters in the objective function to reduce the violation of the predetermined thresholds.

In the first method, the nonconvex nature of the DVCs leads to a nonlinear model (Deasy 1997). We can handle this nonlinearity by introducing binary variables, which results in a large mixed integer problem (MIP) (Lee et al. 2003, Preciado-Walters et al. 2004). Despite many improvements to the MIP formulation Halabi et al. (2006), the FMO problem with DVCs is nonconvex and NP-hard, i.e., the exact solution cannot be obtained in a polynomial computational time using current computing methods (Tuncel et al. 2012). Romeijn et al. (2003) proposed a linear approximation of the DVCs based on the Conditional Value-at-Risk (CVaR) in FMO. Then, Romeijn et al. (2005) developed a column generation based algorithm for IMRT treatment planning and used the CVaR constraints in the model. However, this approach drastically increases the number of constraints and consequently the computational time.

The second method automatically adjusts the model parameters in the objective function to meet the predetermined DVH criteria (Breedveld et al. 2007, Breedveld et al. 2009, Voet et al. 2013). Wu and Mohan (2000) employed a gradient optimization method for the FMO model and considered a simple algorithm adjusting voxel weights in the objective function based on dose-volume histogram. Li et al. (2013) improved the previous work by a two-step approach for FMO problem: In the first step, the organ weights in the quadratic objective function are roughly adjusted; and in the second step, the voxel weighting factors are adjusted based on the DVH curves. In the same line of research, Zarepisheh et al. (2014) have proposed an algorithm that automatically adjusts the FMO parameters to minimize the distance between the DVHs for the entire plan and the reference DVHs. They iteratively navigate the Pareto surface and project the plan corresponding to the reference DVHs onto that surface. Recently, fuzzy inference systems also have been used for the FMO problem (Dias et al. 2016).

To the best of our knowledge, most studies on DVH-based re-optimization have focused on FMO. The current work is on VMAT and such an approach could be effective because of the large scale of the VMAT problem. Moreover, in this paper, we take advantage of Direct Aperture Optimization (DAO) approach, incorporating the sequencing and intensity optimization using column generation (Men et al. 2007, Peng et al. 2012, Mahnam et al. 2017). To this end, we use the iterative procedure of column generation to automatically handle dose-volume criteria in VMAT treatment planning. Thus, the deliverability of the plan is considered at the same time of weight adjustment; Then, both the dosimetric-derived nonconvexity, i.e., the DVH criteria, and

the hardware-derived nonconvexity, i.e., the MLC apertures, are taken into account, simultaneously. We test several strategies, in which the weight of the structures and voxels in the cost function are adjusted at the same time the apertures are generated.

2. Methods and materials

2.1. VMAT optimization model

In this section, we briefly describe our column generation-based heuristic algorithm for VMAT treatment planning (Mahnam et al. 2017). In this technique, we decompose the complicated and nonlinear VMAT optimization model into two linear sub-problems, which iteratively generate and select apertures that are expected to improve the objective function. We focus on treatment plans with a single gantry rotation, which results in less total treatment time and required number of monitor units. However, this approach could easily be generalized to take into account multiple gantry rotations if required in practice.

2.1.1. Notation. We discretize each structure s of the patient into small cubic volume elements called *voxels*, $\mathcal{V}_s$, and denoted $\mathcal{V}_T$ and $\mathcal{V}_N$ for tumorous and normal tissues. Each beam is decomposed into a rectangular grid of *beamlets*, I. A beamlet is on if it is not blocked by either the leading or trailing MLC leaf, and the relative motion of the leaves controls the intensity. The estimated dose received by voxel j from beamlet i at unit intensity is given by the dose-influence matrix (D_{ij}), in Gy/MU.

The continuous dose delivery is discretized over a finite number of *sectors*, H, by changing the angle of the beam, with typically 2°-spaced beam angles. Each sector is associated with an aperture A specifying the position of the MLC trailing (left) and leading (right) leaves and the dose rate ρ (in MU/s). Another variable is the gantry speed in sector h, ν_h. Without loss of generality, we use its inverse as the sector time, t_h, to simplify the model.

The absorbed dose is estimated by the product of dose intensity and time, which makes the model nonlinear. To avoid this nonlinearity, we replace $\rho_h\, t_h$ by a new variable called the *fluence rate*, γ_h. We assume that the dose absorbed by a given voxel can be determined by summing the dose from each of the beamlets comprising the aperture. Thus, the dose received at voxel j, z_j, is calculated as $z_j = \sum_{h\in H} D_j(A_h)\,\gamma_h$, where $D_j(A_h)$ denotes the total dose received by voxel j of aperture h, A_h. We measure the treatment quality via a convex objective function with a piecewise quadratic voxel-based penalty as follows (Romeijn et al. 2005, Peng et al. 2012, Papp and Unkelbach 2014):

$$f(z) = \sum_{s\in S}\sum_{j\in\mathcal{V}_s} \underline{w}_j\,[\underline{d}_s - z_j]_+^2 + \overline{w}_j\,[z_j - \overline{d}_s]_+^2 \tag{1}$$

where $[\bullet]_+$ denotes $\max\{0,\bullet\}$ and $\underline{d}_s$ and $\overline{d}_s$ are prespecified lower and upper dose thresholds for structure s. Moreover, $\underline{w}_j$ and $\overline{w}_j$ are the weights for the underdose and overdose in voxel j, respectively. The weights could be equal for all voxels in the

same structure or be independent. We adjust these parameters in Section 2.2 to obtain clinically acceptable treatment plans.

2.1.2. Column generation. In this model, each column k is a partial arc made up of the apertures, A_h^k, in a sequence of sectors from sector h_s^k to h_f^k, H^k. The procedure starts with a subset of initial columns completely surrounding the patient. The following two sub-problems are then solved repeatedly until no improving column is available:

- RMP: Given a set of columns ($K' \subseteq K$), we select the best subset that covers all the sectors, optimizing the intensities, gantry speed, and dose distribution.
- SP: Given the extra voxel information from the RMP and the effects of the beamlets on the dose distribution, we generate promising columns and add them to the RMP to improve its objective function.

Restricted master model: In the RMP, we determine the best combination of columns around the patient and optimize the corresponding fluence rates. We define the binary variable y: $y^k = 1$ if and only if column k is selected. The dose in each sector h is then $D_h(A_h^k) y^k \gamma_h$. To linearize the model, we assume a constant fluence rate through the covered sectors of column k, denoted γ^k, and we introduce a constraint to restrict it based on y^k. The formulation of the restricted master problem is described in Appendix Appendix A.

Although the fluence rate is fixed for the sectors in a given column, it can change between columns. Moreover, the gantry speed can change between sectors. To make CG more efficient in this phase, we use the voxel aggregation algorithm of Mahnam et al. (2017) to cluster similar voxels and decrease the number of constraints.

After selecting the final apertures at the end of CG, we use a post-optimization (PO) model to determine the sector-based fluence rates. This model considers all the voxels and restricts changes in the fluence rate between adjacent sectors.

Subproblem(SP): In the subproblem, also called the pricing problem, we use the dose distribution z to compute the potential effect of each beamlet $i \in I$ in sector h for an increase of one unit of intensity:

$$\lambda_i^h = \sum\nolimits_{j \in \mathcal{V}} -\nabla f(z_j)\, D_{ij}^h, \tag{2}$$

where ∇f is the gradient of the objective function f. We then use a graph approach to determine the position of the leading and trailing leaves in the new arc. Each node defines a feasible arrangement of MLC leaves, and each edge determines the feasibility between two adjacent nodes. The cost of node n in sector h is based on the potential effects of the open beamlets, I_n^o, as follows:

$$c_n^h = \sum\nolimits_{i \in I_n^o} \lambda_i^h. \tag{3}$$

The network takes into account the MLC constraints by eliminating infeasible graph nodes and edges. These constraints avoid collisions of leaves with $\Delta^{\min} > 0$ and also

ensure that the maximum tip difference is in the specified range $\Delta^{\max}$. Moreover, leaf movements between adjacent sectors are restricted based on the maximum leaf speed. Finally, we determine the best MLC aperture for a given range of sectors by a polynomial-time shortest-path algorithm and add the new columns to the RMP if the objective value is negative.

Greedy Heuristic: As mentioned, the RMP is a MIP because of the binary variables y^k. At the beginning of the algorithm, we relax the binary requirement, and so the y^k variables are usually fractional. To find a feasible plan in a reasonable time, we fix the lower bound of the column with the largest fractional part to 1 at each CG iteration and remove the conflicting partial-arcs. Also, we keep other generated columns in the model for the next iterations.

More details about the CG-based heuristic and its efficiency can be found in our previous publication Mahnam et al. (2017).

2.2. Adjustment approach

In this section, we formulate the adjustment model for the structure and voxel weight vectors, and also the adjustment procedure embedded in the column generation algorithm.

2.2.1. Weight adjustment. Let $\mathcal{F}$ be the feasible solution space of model RMP and f the voxel-based objective function. We formulate the treatment planning problem using the weighted-sum method to convert the multicriteria DVH objectives into a single-objective optimization problem as follows:

$$\mathbf{P}: \min_{(y,\gamma,t)\in\mathcal{F}} w^\top f(z(y,\gamma,t)) \tag{4}$$

where w is a vector of non-negative weights representing the relative importance of the structures or voxels. For the l^{th} DV objective of structure s with dose value d_s^l, let $V_{d_s^l}$ and $v_{d_s^l}$ denote the desired and actual percentages of the structure volume, respectively.

To implement this general model in the course of column generation algorithm, we first find the treatment plan subject to the delivery constraints at each iteration. We then evaluate its DVH criteria, $\boldsymbol{v}$, and update the weight vector w based on the formulation. This process continues until we find an acceptable DVH or the stopping criteria are satisfied. The details of the algorithm are provided in subsequent sections.

In the structure-based weight vector, all voxels in a structure have the same weight in the objective function, while in the voxel-based adjustment, the weights are independent. The solution space of the model P is larger in the second approach, which makes the problem more complicated but also more flexible.

Structure-based weight vector: In this case, it suffices to find the underdose, w_s^-, and overdose, w_s^+, weighting factors of structure s. To adjust the weights during the CG, we

use the formulations inspired by Li et al. (2013), which increase the weight of structures corresponding to the violations from the prescribed thresholds. Let L_s^+ be the DVH criteria for the overdose in structure s. The total overdose is as follows:

$$\delta A_s^+ = \sum_{l \in L_s^+} \max(0, v_{d_s^l} - V_{d_s^l}). \tag{5}$$

Similarly, we can compute the total underdose of structure s, δA_s^-. We update the organ weights at each iteration of CG for the restricted mater problem (RMP) based on the weights in the previous iteration and the ratio of the overdose (δA_s^+) or underdose (δA_s^-) in structure s to the total overdose and underdose in all structures. This formulation is shown for overdose weighting factor, w_s^+, in Equation (6) and the overdose weighting factors can be computed similarly.

$$w_{s,k+1}^+ = \alpha\, w_{s,k}^+ \,(1 + \frac{\delta A_s^+}{\sum_{s \in S} \delta A_s^+ + \delta A_s^-}) \tag{6}$$

where the parameter α controls the effectiveness of the weight adjustment. This adaptive parameter has a relatively small value in the initial iterations and increases at a constant rate as the algorithm proceeds. It helps to adjust the treatment plan, especially in the PO phase, where the values of the overdose and underdose are small.

Voxel-based weight vector: In this approach, the voxel weights are the same for each structure at the beginning of the algorithm but are adjusted independently during the CG according to the treatment plan. However, the DVH criteria are cumulative measures, in which there is no direct relationship between a certain voxel and a DVH goal. Let $\pi(z^s)$ be a permutation of the voxel doses in structure s, and let $\widetilde{\pi}(d^s)$ be the permutation that sorts z^s in nondecreasing order. Zarepisheh et al. (2014) have shown that $\widetilde{\pi}(z^s)$ yields the best approximation to the DVH goals among all permutations of z. For the l^{th} DV objective in structure s, denoted $(d_s^l, V_{d_s^l})$, we obtain $\widetilde{\pi}(z^s)$ and for each voxel j we modify the weight at iteration $k+1$ as follows:

$$w_{j,s}^{k+1} = \begin{cases} \alpha\, w_{j,s}^k \frac{d_s^l}{z_{j,s}} & s \in T, V(\widetilde{\pi}(z_{j,s})) \leq V_{d_s^l}, z_{j,s} \leq d_s^l \\ \alpha\, w_{j,s}^k \frac{z_{j,s}}{d_s^l} & s \in N, V(\widetilde{\pi}(z_{j,s})) \geq V_{d_s^l}, z_{j,s} \geq d_s^l \\ w_{j,s}^k & \text{o.w.} \end{cases} \tag{7}$$

where $V(\widetilde{\pi}(d_j^s))$ is the percentage of the organ receiving dose z_j^s or more in the sorted version of the current solution. Figure 1 shows a sample of this criterion for $V30 \leq 80\%$ in a normal structure and the voxel weight adjustment area. If there is more than one goal point in the structure, we consider the penalty for voxel j based on the closest DVH reference point.

The difference between the actual and desired DVH criteria, especially in the final iterations of the algorithm, is usually insignificant. For example, $V30 = 80.01\%$ while the desired volume is 80%. In these cases, the weight of just few voxels will be modified during the weight adjustment, and the unsatisfied DVH goal will not be improved. Thus, in addition to α, which controls the intention of the weight adjustment, we need a parameter to increase the range of the affected voxels when the actual and desired criteria are very close. To affect an additional $\epsilon\%$ of the voxels, we adjust the desired dose d_s^l in the conditions of Equation (7) to $z_{j,s} \leq (1+\epsilon)\, d_s^l$ and $z_{j,s} \geq (1-\epsilon)\, d_s^l$ for tumorous and normal voxels, respectively. Figure 1 shows a DVH objective $(d_s^l, V_{d_s^l})$, the voxel weight adjustment area, and the $\epsilon\%$ extension in the range of affected voxels.

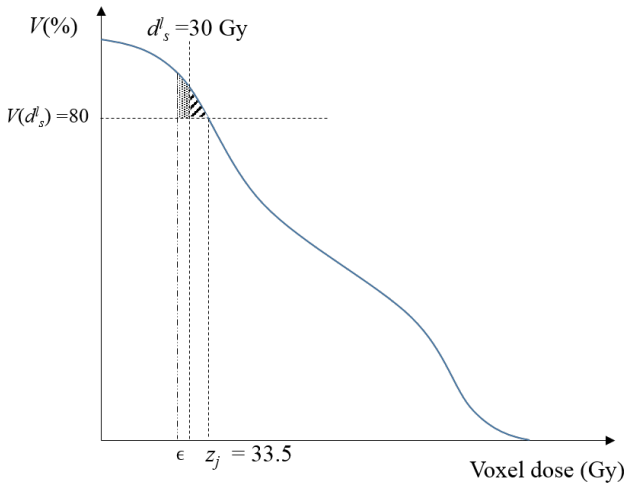

Figure 1. Voxel weight adjustment for $V30 \leq 80\%$ in a normal tissue. The voxel doses (z_j) are sorted in nondecreasing order on the horizontal axis, and the percentage of the organ is indicated on the vertical axis. The hatched area shows the penalized voxels. The $\epsilon\%$ extension in the range of affected voxels is shown in the dotted area.

2.2.2. Proposed strategy. In the proposed CG, we dynamically update the weight vector. To this end, we must determine (1) the adjustment approach, (2) the best iteration for the adjustment, (3) a DVH evaluation heuristic, and (4) the post-optimization (PO). These strategies are explained in more detail below.

Adjustment approach: We first choose between structure-based adjustment (SA-CG) and voxel-based adjustment (VA-CG), explained in Section 2.2.1. The former has a smaller solution space and the latter has more flexibility.

Adjustment iteration: We perform the adjustment every p iterations. For small values of p, the objective function will change frequently, and our method approximates a greedy algorithm. On the contrary, when p is large, the weight adjustment will be less effective.

DVH evaluation: As explained in Section 2.1.2, the variables associated with the

columns, y^k, are fractional at the beginning of the CG procedure and are gradually fixed to 0 or 1. We developed two simple heuristics to evaluate the quality of the treatment plan during the algorithm: the partial relaxed plan (PRP) and the greedy plan (GP). In PRP, column variables in the solution may be fractional, and the doses at the voxels are based on the partial plan. Due to the fractional values, this estimation is usually optimistic. In GP, we fix the column with the largest value at each sector to 1 to make a complete feasible solution. We then solve the model again and evaluate the DVH criteria.

Post-optimization (*PO*): At the end of the column generation procedure, we can continue the re-optimization process. In the PO phase, the apertures are fixed, but the fluence rate is sector-dependent, i.e., the fluence rates in sectors are independent, but we restrict the changes between adjacent sectors. However, because it considers all the voxels, the PO model is large and time-consuming to solve. We perform a maximum of 20 iterations in the PO phase, updating the weights between the iterations. We terminate the algorithm when the DVH criteria are satisfied.

Figure 2 depicts a flowchart of our CG procedure with weight adjustment. To find the best strategy, we tested several approaches and parameter settings; see Section 3.

2.3. Materials

We evaluate the efficiency of the proposed algorithm on two clinical cases from the CORT data set (Craft et al. 2014): a prostate (P) patient and a head-and-neck (H&N) patient. The prostate case has two target volumes with different prescription, PTV-56 and PTV-68, and six organs at risk: the bladder, rectum, left and right femoral heads, prostate bed, and penile bulb. The head-and-neck case has three target volumes, PTV-56, PTV-63, and PTV-70, and four organs at risk: the brainstem, spinal cord, and right and left parotids. Doses of 68 Gy in the prostate case and 70 Gy in the head-and-neck case were prescribed in 2 Gy per fraction. Then, the treatment plans were optimized for 34 and 35 fractions, respectively. The parameters for the two cases are listed in Table 1. As one can see, there are more voxels in the prostate case and more beamlets in the head-and-neck case. From the mathematical point of view, the former has more constraints, and the latter has more potential columns. Therefore, the algorithm is analyzed in terms of both aspects. Also, the machine parameters, typically considered in the literature (Craft et al. 2014), are listed in Table 2.

In both cases, the 360 degrees around the patient are covered by 180 equally spaced sectors. Based on the sensitivity analysis for the arc length in our previous work (Mahnam et al. 2017), we take into account 12° per arc, i.e., 30 arc segments.

We use standard DVH reference points based on those in the literature and the advice of a medical physicist; see Table 3. The goal is to ensure that 95% of the target volumes are covered by 100% of the prescribed dose while minimizing the dose to normal tissues. Moreover, to avoid pockets of high doses (hot spots) within the target, high dose values are restricted.

Table 1. Parameters of clinical cases

	Prostate (P)	Head & neck (H&N)
Total # beamlets	25,404	203,765
Beamlet size (cm)	1×1	0.5×0.5
Voxel resolution (mm)	3, 3, 3	3, 3, 5
# Target voxels	9,491	25,388
# Body voxels	690,373	251,893
Prescribed dose (Gy)	68	70
# Fractions	34	35

Table 2. VMAT machine parameters

Maximum leaf speed, ν_l^U	3 cm/s
Gantry speed, ν_g	1–6°/s
Maximum dose rate, ρ^U	600 MU/min
Maximum fluence change, Δ_γ	2 MU/s
Maximum change in sector time, Δ_t	2 s

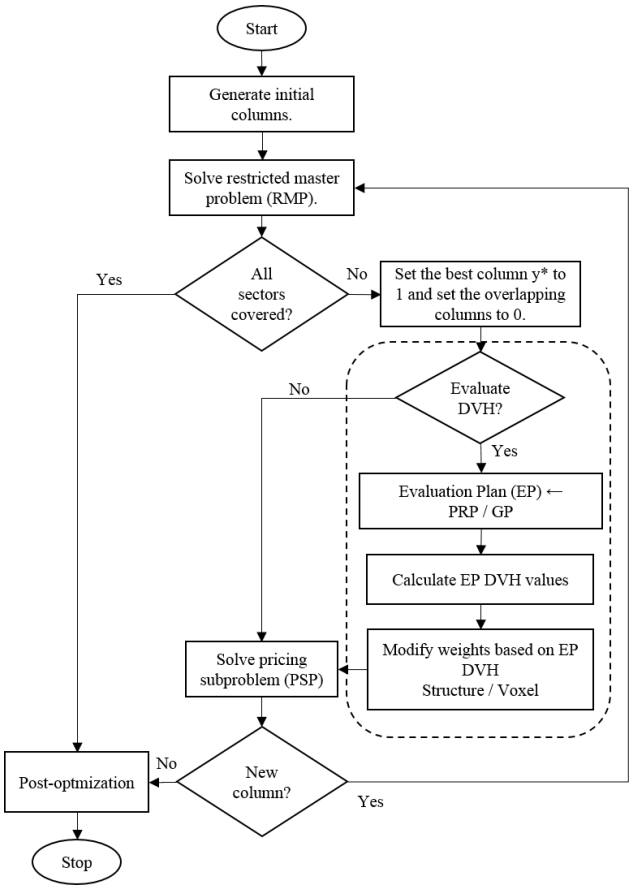

Figure 2. Flow chart of CG heuristic with weight adjustment. The adjustment process is determined by a dashed outline.

Table 3. Treatment plan dose-volume criteria

Prostate (P)		Head-and-neck (H&N)	
Structure	Measure	Structure	Measure
PTV-56	V56 $\geq$ 95%	PTV-56	V56 $\geq$ 95%
PTV-68	V68 $\geq$ 95%	PTV-63	V63 $\geq$ 95%
	V74.8 $\leq$ 1%	PTV-70	V70 $\geq$ 95%
Rectum	V30 $\leq$ 70%		V76.3 $\leq$ 1 %
	V50 $\leq$ 50%	Rt. Parotid	V50 $\leq$ 20%
	V65 $\leq$ 25%	Lt. Parotid	V50 $\leq$ 20%
Bladder	V40 $\leq$ 60%	Spinal cord	V48 $\leq$ 1%
	V65 $\leq$ 30%	Brainstem	V60 $\leq$ 1%
Femoral heads	V50 $\leq$ 1 %		

3. Results

We implemented the algorithms in C++ and used IBM ILOG CPLEX 12.6.2 for the mathematical models. The computational experiments were run on a 2.67 GHz Intel(R) Xeon(R) E7-8837 Linux workstation. To improve the efficiency of the algorithm for the subproblem, we used parallel programming techniques with a maximum of 10 threads. We solved the quadratic RMP at each iteration using the CPLEX Barrier Optimizer, which is based on an interior-point method.

To assess the effectiveness of the proposed algorithm in the prostate and head-and-neck cases, we randomly generated 15 scenarios for the initial weights of the structures in each case. For instance, the weight of Bladder in the prostate case in one scenario is 0.2 while it is 0.4 in another scenario. This allows us to analyze the robustness of the algorithm to initial parameters and its adaptability to different cases and priorities. Then, we tested the generated scenarios on 15 strategies, where each strategy is a combination of an adjustment approach (`adjust. method`), the frequency of the weight adjustment ($\boldsymbol{p}$), and a DVH evaluation heuristic (`DVH eval.`).

The adjustment approach is structure- or voxel-based, and we adjust the weights every $p = 1$, 5, or 10 iterations. Moreover, the DVH evaluation heuristic is Partial Relaxed Plan (PRP) or Greedy Plan (GP). In addition to weight adjustment during the column generation, we perform the DVH-based re-optimization for a maximum of 20 iterations in the PO phase.

3.1. Prostate case

The details of the strategies and the results are summarized in Table 4. In the first strategy, so-called *simple VMAT*, we test the column-generation based heuristic without weight adjustment neither during CG nor the PO phase (Mahnam et al. 2017). Then, for each adjustment approach, we take into account one strategy, so-called *PO-Adjustment*, with adjustment only for the post-optimization iterations and six strategies with weight adjustment both during the CG and PO phases.

Table 4. The results of proposed strategies in the prostate case.

Strateg.	adjust. method	p	DVH eval.	# plans during PO 1	5	10	15	20	avg. iter.	avg. deliv. time (min)
S-P-1	Simple CG	N/P	N/P	3	-	-	-	-	-	3.02
S-P-2	SA-PO	N/P	N/P	3	7	10	11	13	8.40	3.07
S-P-3	SA-CG	1	PRP	8	11	14	14	14	3.73	3.14
S-P-4		5	PRP	4	10	13	13	14	5.73	3.13
S-P-5		10	PRP	4	10	13	13	14	5.40	3.07
S-P-6		1	GP	6	9	11	13	13	6.33	3.12
S-P-7		5	GP	6	9	12	13	13	6.40	3.16
S-P-8		10	GP	4	10	14	15	-	4.46	3.13
S-P-9	VA-PO	N/P	N/P	1	13	15	-	-	2.33	3.07
S-P-10	**VA-CG**	**1**	**PRP**	**13**	**15**	-	-	-	**1.27**	**3.20**
S-P-11		5	PRP	6	14	15	-	-	2.47	3.16
S-P-12		10	PRP	7	13	13	13	13	4.00	3.05
S-P-13		1	GP	2	13	15	-	-	3.27	3.06
S-P-14		5	GP	3	14	14	15	-	2.87	3.10
S-P-15		10	GP	7	15	-	-	-	1.60	3.09

The cumulative number of instances with acceptable plans at the end of iterations 1, 5, 10, 15, and 20 in the PO phase are reported in the column `# plans during PO`. The `avg. iter.` column gives the average number of PO iterations, and the `avg. deliv. time` column gives the average delivery time (in minutes).

The results indicate that the simple strategy S-P-1 finds just three clinically acceptable plans out of 15 and takes about 6.51 min. The main challenge is to cover

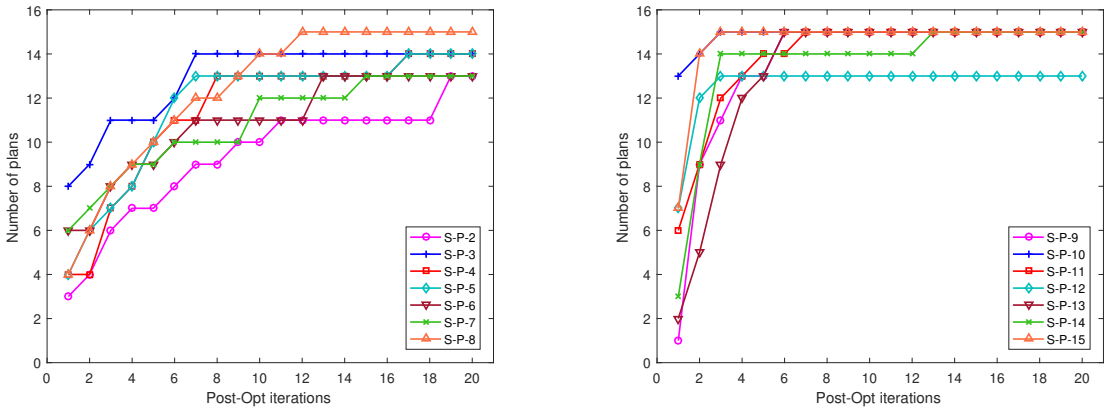

a) Structure-based adjustment approach b) Voxel-based adjustment approach

Figure 3. Number of clinically acceptable plans for the prostate case during the post-optimization iterations: (a) structure-based adjustment strategies, SA-PO and SA-CG, (b) voxel-based adjustment strategies, SA-PO and SA-CG.

PTV-56 and PTV-68 at their prescribed doses while satisfying the upper thresholds for the rectum and the target volumes. As a PO-Adjustment strategy, S-P-2 use CG to generate efficient apertures but adjust the structure weights in PO iterations. Strategies S-P-3 to S-P-8 use the structure-based adjustment also embedded in column generation (SA-CG) and find up to 13-15 plans gradually during the PO phase. Similar to S-P-2, strategy S-P-9 modifies the weight vector only in PO iterations but based on voxel adjustment. Strategies S-P-10 to S-P-15 with voxel-based adjustment approach during the CG and PO procedures (VA-CG) find acceptable plans for 14-15 instances.

To compare the trends of the structure- and voxel-based strategies during PO phase, Figure 3 indicates the cumulative number of obtained acceptable plans at each iteration. It can be seen that the VA-CG strategies are closer to the top left side of the diagram, i.e., more plans in fewer iterations. It shows that the VA-CG approach finds 89 plans in at most three PO iterations; this value is only 55 for SA-CG. S-P-10 finds plans for all the instances in 7.18 minutes on average and at most two PO iterations (the average is 1.27). It requires about 10% more computational time than simple VMAT, which is negligible in comparison with the improvement. Also, the obtained average delivery time is about 3 minutes in different strategies.

Moreover, Figures 3a and 3b show that the results of Strategies S-P-2 and S-P-9, modifying the weight vectors only in the PO phase, are less efficient than similar approaches. These results gain a better insight into the value of the integration of DVH criteria in column generation. We conclude that adjusting the weight during the CG leads to more clinically acceptable plans within less computational time.

Figure 4 illustrates the DVHs for an instance solved by S-P-1 (simple VMAT) and S-P-10 (VA-CG) as the best found strategy. The plans for this instance, both are obtained in the first PO iteration of S-P-1 and S-P-10, respectively. It can be seen that the S-P-1 plan does not deliver the prescribed doses to the target volumes and the criteria associated to the femoral heads and target overdose are close to the pre-determined limits. However, the S-P-10 plan satisfy all the requirements for normal and target volumes.

3.2. Head-and-neck case

In the large and challenging head-and-neck case, the goal of the treatment plan is to cover all three targets while avoiding hot spots and sparing the parotid glands, spinal cord, and brainstem. Similarly to the prostate case, we compare the structure- and voxel-based weight adjustment approaches, PRP and GP evaluation heuristics, the frequency of the weight adjustment for $p = 1, 5$ and 10 in 15 randomly generated weight scenarios in the range of user experience. In total, we test 15 strategies; the results are summarized inTable 5.

The simple VMAT algorithm, S-HN-1, finds no acceptable treatment plan, but the proposed algorithm finds admissible plans for 14 out of 15 (93.33%) instances in three strategies. S-HN-3 to S-HN-8 strategies, using the SA-CG approach, find 11-14

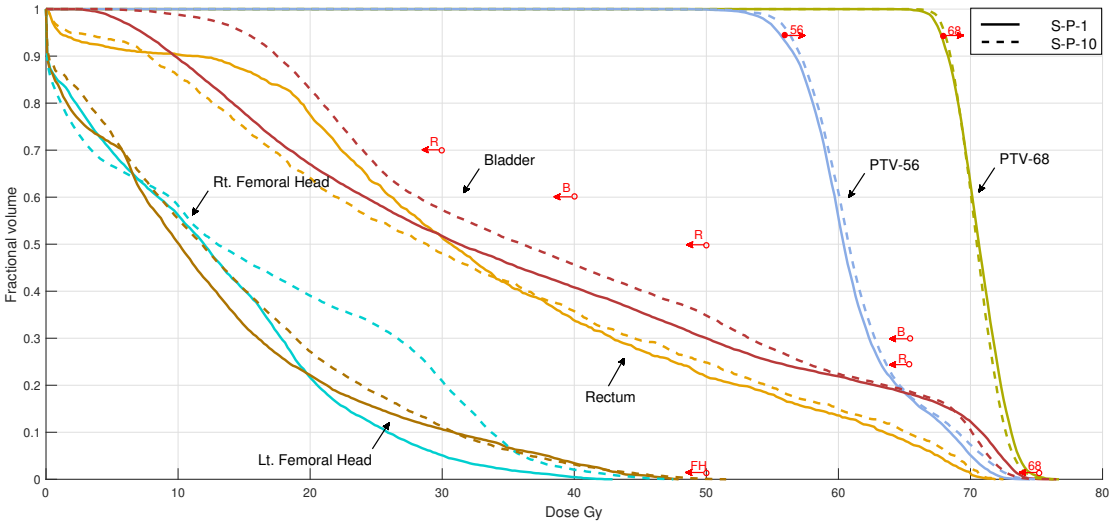

Figure 4. DVH of the prostate treatment plan for instance #1 in two strategies: S-P-1 (solid line) as simple VMAT and S-P-10 (dashed line) as the best found approach. Empty circles (○) indicate overdosage and solid circles (●) indicate underdosage DVH criteria. An arrow with a letter above indicates the direction of allowed curves for the specified structure. "B" is the bladder, "R" the rectum, "FM" the femoral heads; "56" indicates PTV-56 and "68" indicates PTV-68.

Table 5. The results of proposed strategies in the head & neck case

Strateg.	adjust. method	p	DVH eval.	# plans during PO 1	5	10	15	20	avg. iter.	avg. deliv. time (min)
S-HN-1	Simple CG	N/P	N/P	0	-	-	-	-	-	2.62
S-HN-2	SA-PO	N/P	N/P	0	0	5	7	10	14.47	2.62
S-HN-3	SA-CG	1	PRP	0	5	9	11	11	10.47	2.62
S-HN-4		5	PRP	0	1	8	12	14	12.20	2.62
S-HN-5		10	PRP	0	7	9	10	11	10.00	2.61
S-HN-6		1	GP	0	2	8	11	11	11.33	2.63
S-HN-7		5	GP	0	2	5	9	12	13.40	2.62
S-HN-8		10	GP	0	3	8	12	13	10.60	2.63
S-HN-9	VA-PO	N/P	N/P	0	9	11	11	11	8.27	2.62
S-HN-10	**VA-CG**	**1**	**PRP**	**0**	**12**	**12**	**14**	**14**	**5.07**	**2.62**
S-HN-11		5	PRP	0	9	12	14	14	6.07	2.63
S-HN-12		10	PRP	0	9	11	12	12	7.87	2.62
S-HN-13		1	GP	0	5	6	10	11	11.53	2.63
S-HN-14		5	GP	0	9	10	12	13	7.87	2.63
S-HN-15		10	GP	0	6	9	10	11	10.53	2.61

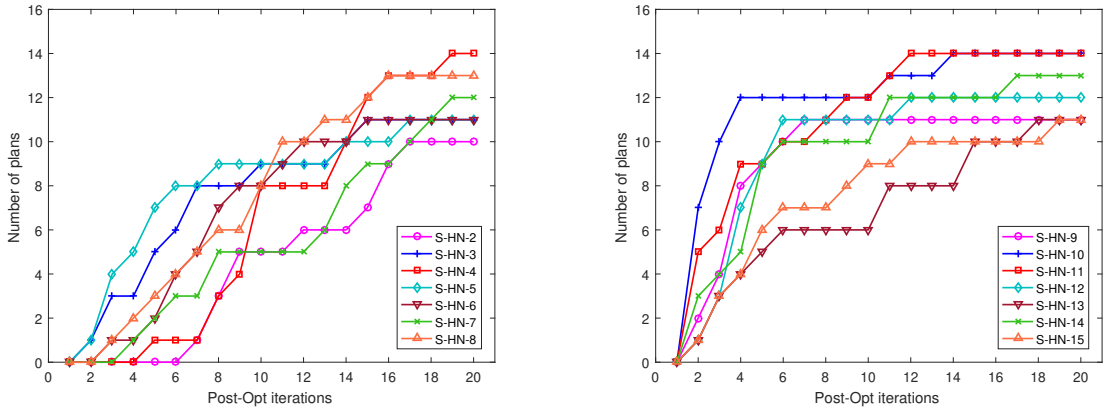

a) Structure-based adjustment approach b) Voxel-based adjustment approach

Figure 5. Number of clinically acceptable plans for the head-and-neck case during the PO iterations: (a) structure-based adjustment strategies, SA-PO and SA-CG, (b) voxel-based adjustment strategies, VA-PO and VA-CG.

acceptable plans during the PO iterations. This number is the same for the VA-CG approach, strategies S-HN-10 to S-HN-15. To differentiate between two approaches, we take into account the first 5 PO iterations which results in 20 and 50 acceptable plans for SA-CG and VA-CG, respectively. Figures 5a and 5b indicate the number of acceptable plans at each iteration for the SA-CG and VA-CG strategies. The comparison of two graphs shows clearly that VA-CG is significantly more efficient than SA-CG. S-HN-10 has the best performance: 14 acceptable plans found while the average computational time is 38.48 minutes. This strategy uses PRP heuristic in every CG iteration and solves the instances in an average of 5.07 PO iterations. The average delivery time is about 2.62 ± 0.01 minutes and robust for different strategies.

Furthermore, S-HN-2 and S-HN-9, which perform the adjustment only in the post-optimization phase, are among the least efficient strategies. Moreover, it can be seen that no acceptable plan was found in the first iteration of the PO phase because of high complexity of the case. However, the algorithm could adapt rapidly and reach an acceptable plan.

Figure 6 compares the DVHs for one of instances solved by S-HN-1 (simple VMAT) and S-HN-10 as a VA-CG approach. It can be seen that S-HN-1 fails to cover PTV-63 and also does not satisfy the tumor overdose criterion, $V76.3 \leq 1\%$. Also, the criteria associated to left and right parotids are close to their limit, $V50 \leq 20\%$. However, S-HN-10 finds an acceptable plan in the second PO iteration. The tail of PTV-63 and PTV-70 have some overlapping parts because of the multi-organ voxels and inaccuracy at the boundaries in both targets.

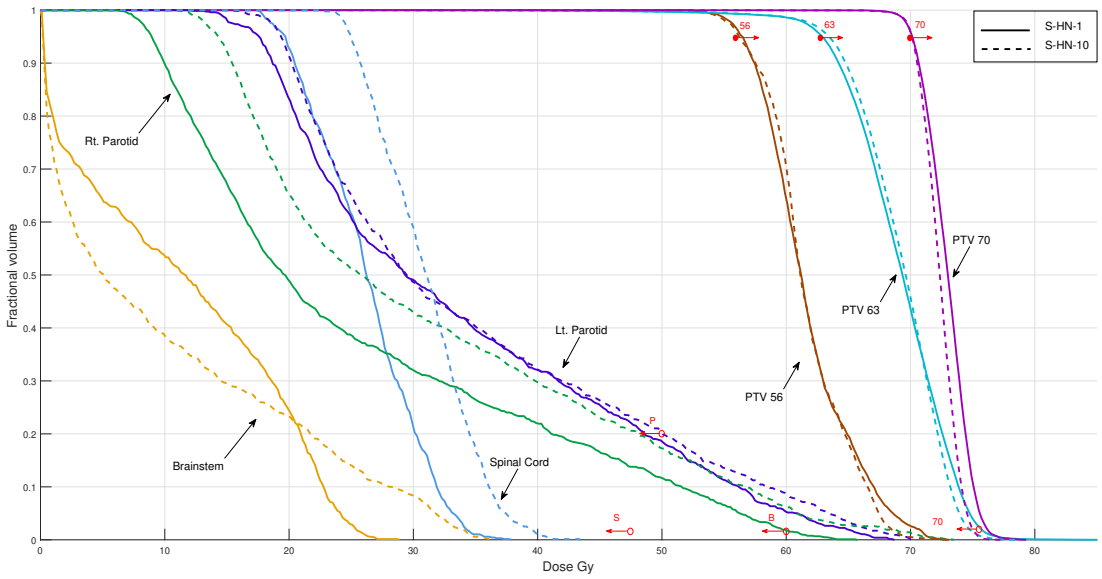

Figure 6. DVH of the head-and-neck treatment plan for instance #9 in two strategies: S-HN-1 as the simple VMAT (solid line) and S-HN-10 as the best obtained approach (dashed line). Empty circles (○) indicate overdosage and solid circles (●) indicate underdosage DVH criteria. The arrow with a letter above indicates the direction of allowed curves for the specified structure. "B" is the brainstem, "S" the spinal cord, and "P" the parotids; "56" indicates PTV-56, "63" indicates PTV-63, and "70" indicates PTV-70.

4. Discussion

The main difficulty in VMAT optimization is the large number of potential apertures and voxel-based constraints which does not allow additional DVH based constraints in the model. Therefore, to integrate the DVH criteria in the column generation technique, we need to find an efficient strategy that automatically obtains acceptable plans. To this end, we have implemented two adjustment approaches: structure-based and voxel-based. The former has a smaller solution space; the latter has more flexibility. We tested our approach on a prostate and a head-and-neck case. The simple VMAT optimization technique (Mahnam et al. 2017) found three plans in the prostate case (out of 15 scenarios with random initial weight vectors) and none in the head-and-neck case. The proposed algorithm could find the acceptable plans for most of instances in both cases which confirms its advantage over the simple VMAT optimization technique.

The voxel-based adjustment (VA-CG) was more successful even with a more complicated solution space. In the prostate case, S-P-10 found plans for all instances with an increase of just 10% in the computational time and 3 PO iterations. The results in the head-and-neck case confirm this conclusion. The best strategy was S-HN-10, finding acceptable plans for 93.3% of instances. The average of PO iterations

to achieve an acceptable plan for all 15 instances is 5.07 iterations with an average computational time of 38.48 minutes.

The best strategies, S-P-10 and S-HN-10, had a high frequency of adjustment during the column generation process. This indicates that the integration is effective in improving the results and the adjustment is usefully employed. In both cases, PRP could find satisfying evaluations of DVH in less computational time than GP. The difference between the average PO iterations by S-P-9 (2.33) and the number found by S-P-10 (1.27) shows more efficiency in S-P-10, in which the DVH is evaluated inside CG frequently. In the larger head-and-neck case, there is an even greater difference between S-HN-9 and S-HN-10, such that the the number of acceptable plans found by S-HN-10 is 14 out of 15 and this number found by S-HN-9 is 10. These comparisons show the value of the integration of the weight adjustment procedure inside the CG algorithm rather than the PO-Adjustment approach.

From the dosimetry point of view (Figures 4 and 6), the target volumes are barely covered in both cases. This is likely due to the structure of column generation technique, which starts from no column, as the best plan for normal tissues, and gradually adds columns to cover the target volumes. The advantage of this approach is that it controls the dose to normal tissues.

In terms of computational time, the extra tasks of DVH evaluation and weight adjustment increase the CPU time in automatic VMAT in comparison to simple VMAT. However, it is negligible as shown in the best obtained strategies, S-P-10 and S-HN-10. We believe that the symmetry of the model is one of the main causes of its complexity, and the weight adjustment breaks the symmetry and consequently decreases the computational time. Moreover, the number of PO iterations to find an acceptable plan decreases when we perform DVH evaluation during the CG. Therefore, we can find better treatment plans with minor additional computational time.

Finally, to have an idea of the efficiency of the proposed algorithm in comparison to a commercial software, a treatment plan is designed by an expert for the prostate case with Pinnacle. The DVH diagram of the plan is shown in Figure 7. This DVH is obtained from a treatment plan with double gantry rotation in about 20 minutes computational time. The other assumptions and parameters are the same as shown in Table 2. The computational time in our plan is less, 7.18 minutes, and at the same time, the quality of the diagrams, especially for the healthy tissues is significantly better. As shown, the DVH obtained from Pinnacle is not acceptable due to high dose to Rectum (V30 $> 70\%$), overdosage in PTV-68 (V74.8 > 1 %) , and not enough coverage to PTV-56 (V56 < 95 %). This single case does not allow us to draw any firm conclusion regarding the efficiency of the proposed algorithm in comparison to a commercial software. In addition, to fully assess the potential of this idea in the context of existing clinical software, we would need to have access to the core algorithm of these software, which is obviously not possible. However, we believe this shows, in a limited way, that our model and our algorithm can provide state-of-the-art results and they could possibly be used to improve existing software.

In sum, the advantages of the proposed algorithm in comparison to most studies in the literature and commercial software are as follows:

- To the best of our knowledge, most studies and software take into account DVH criteria as constraints in the mathematical model which makes the model non-linear or large and consequently more costly to solve.
- The DVH based models are mostly considered only in FMO while the current work is on VMAT and such an approach could be effective because of the large scale of the VMAT problem.
- The proposed algorithms integrating DVH constraints and direct aperture optimization are in large-scale (Romeijn et al. 2005) and non-applicable in practice for VMAT.
- In this paper, we incorporate the sequencing and intensity optimization using column generation. Thus, the deliverability of the plan is considered at the same time of weight adjustment; Then, both the dosimetric-derived nonconvexity, i.e., the DVH criteria, and the hardware-derived nonconvexity, i.e., the MLC apertures, are taken into account, simultaneously.
- Less trial-and-error in the search for clinically acceptable plans increase the efficiency of the software and also the center.

5. Conclusion

In this paper, we have taken into account both dosimetric and hardware constraints to produce deliverable plans for VMAT treatment planning and also dynamically adjusted the penalty weights of the objective function to automatically obtain clinically acceptable plans. This approach increases the efficiency of the algorithm and consequently decreases the human interventions.

To this end, we integrated structure-based and voxel-based adjustment algorithms in the column generation technique to update the weight vectors based on DVH criteria in the objective function. This approach does not require additional dose-volume constraints in the master model, leading to minimal re-optimization in the PO phase and increasing the efficiency of the treatment planning. We evaluated our approach on a prostate and a head-and-neck case; the former has more voxels (constraints), and the latter has more beamlets (columns). The performance of the proposed voxel-based adjustment in column generation (VA-CG) is significantly better than simple VMAT, without weight adjustment, and also PO-Adjustment approach, considering weight adjustment only in the post-optimization phase. This method does not guarantee to reach all DVH criteria, but makes the VMAT treatment planning more robust to initial parameters during the MLC aperture generation without much additional computing time.

Further work could be carried out with more analysis on a wide range of patients to analyze and improve the efficiency of the algorithm in practice in existing commercial

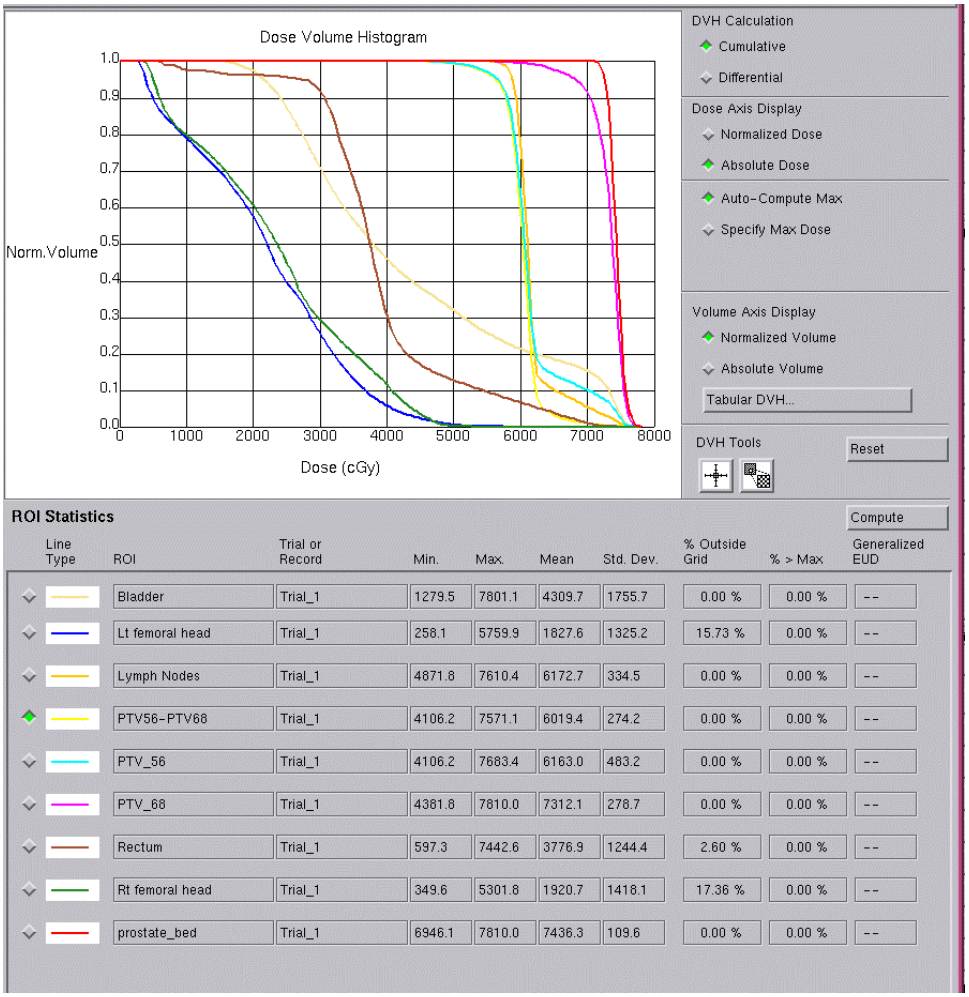

Figure 7. DVH of the prostate treatment plan with commercial software.

software. Moreover, the proposed algorithm considers multiple DVH criteria in the treatment evaluation. It would also be possible to apply this methodology to the whole DVH curve. Future work will also consider the use of graphics processing unit (GPU) to accelerate the method.

Acknowledgments

The authors gratefully acknowledge financial support from the Natural Sciences and Engineering Research Council of Canada (NSERC) and the Vanier Canada Graduate Scholarship program (DVC134707). We also thank Prof. David Craft, Harvard Medical School, who helped us by providing the data, Dr. Marc-André Renaud, McGill University, for helpful comments, and Dr. Martin Hinse, Medical Physicist at Laval Integrated Cancer Centre (CICL), for comparison to commercial sotware. The authors also wish to thank the anonymous referees whose insightful comments have helped us to improve our paper.

Appendix A. Formulation of the master model

The formulation of the restricted master problem is as follows:

$$\textbf{RMP}: \min f(z) \tag{A-1}$$

$$\text{s.t.} \quad z_j = \sum\nolimits_{k\in K'} \sum\nolimits_{h\in H_k} D_{jh}(A_h^k)\,\gamma^k \qquad \forall j \in \mathcal{V} \tag{A-2}$$

$$\sum\nolimits_{k\in K'} b_h^k\, y^k \le 1 \qquad \forall h \in H \tag{A-3}$$

$$\gamma^k \le \Gamma^k\, y^k \qquad \forall k \in K' \tag{A-4}$$

$$\sum\nolimits_{k\in K'} b_h^k\, \gamma^k \le \overline{\rho}\, t_h \qquad \forall\, h \in H \tag{A-5}$$

$$\sum\nolimits_{k\in K'} \tau_{h,h+1}^k\, y^k \le t_h \qquad \forall\, h \in H \tag{A-6}$$

$$\underline{T} \le t_h \le \overline{T} \qquad \forall\, h \in H \tag{A-7}$$

$$y^k \in \{0,1\},\ \gamma^k \ge 0 \qquad \forall k \in K' \tag{A-8}$$

where z_j, the dose absorbed by voxel j, is computed in Constraint (A-2) based on the sectors covered by column k, H_k; the aperture shape, A_h^k; and the column fluence rate, γ^k. In Constraint (A-3) b_h^k indicates the coverage of sector h by column k, and the constraint ensures that each sector h is covered by at most one column. Constraints (A-4) and (A-5) enforce the upper bound on the fluence rate. In constraints (A-4), the fluence rate of each column is restricted to the maximum fluence rate of column k, Γ^k, if selected, based on the maximum dose rate and the minimum gantry speed. In constraints (A-5) the fluence rate at each sector is bounded by the maximum dose rate $\overline{\rho}$ and the sector time. Also, Constraints (A-6) ensure that the time spent at sector h is sufficient to allow the leaf movements to reach the next aperture A_{h+1}^k. Finally, Constraints (A-7) enforce the lower and upper bounds on the sector time.

References

Balvert, M. and Craft, D. (2017). Fast approximate delivery of fluence maps for IMRT and VMAT, *Physics in Medicine and Biology* **62**(4): 1225–1247.

Bedford, J. L. (2009). Treatment planning for volumetric modulated arc therapy, *Medical Physics* **36**(11): 5128–5138.

Bokrantz, R. (2012). Multicriteria optimization for volumetric-modulated arc therapy by decomposition into a fluence-based relaxation and a segment weight-based restriction, *Medical Physics* **39**(11): 6712–6725.

Breedveld, S., Storchi, P. R. and Heijmen, B. J. (2009). The equivalence of multi-criteria methods for radiotherapy plan optimization, *Physics in Medicine and Biology* **54**(23): 7199–7209.

Breedveld, S., Storchi, P. R., Keijzer, M., Heemink, A. W. and Heijmen, B. J. (2007). A novel approach to multi-criteria inverse planning for IMRT, *Physics in Medicine and Biology* **52**(20): 6339–6353.

Bzdusek, K., Friberger, H., Eriksson, K., Hårdemark, B., Robinson, D. and Kaus, M. (2009). Development and evaluation of an efficient approach to volumetric arc therapy planning, *Medical Physics* **36**(6): 2328–2339.

Cao, D., Afghan, M. K., Ye, J., Chen, F. and Shepard, D. M. (2009). A generalized inverse planning tool for volumetric-modulated arc therapy, *Physics in Medicine and Biology* **54**(21): 6725–6738.

Craft, D., Bangert, M., Long, T., Papp, D. and Unkelbach, J. (2014). Shared data for intensity modulated radiation therapy (IMRT) optimization research: The CORT dataset, *GigaScience* **3**: 37–48.

Craft, D., McQuaid, D., Wala, J., Chen, W., Salari, E. and Bortfeld, T. (2012). Multicriteria VMAT optimization, *Medical Physics* **39**(2): 686–696.

Deasy, J. (1997). Multiple local minima in radiotherapy optimization problems with dose–volume constraints, *Medical Physics* **24**(7): 1157–1161.

Dias, J., Rocha, H., Ventura, T., Ferreira, B. and do Carmo Lopes, M. (2016). Automated fluence map optimization based on fuzzy inference systems, *Medical Physics* **43**(3): 1083–1095.

Halabi, T., Craft, D. and Bortfeld, T. (2006). Dose–volume objectives in multi-criteria optimization, *Physics in Medicine and Biology* **51**(15): 3809–3818.

Lee, E. K., Fox, T. and Crocker, I. (2003). Integer programming applied to intensity-modulated radiation therapy treatment planning, *Annals of Operations Research* **119**(1): 165–181.

Li, N., Zarepisheh, M., Uribe-Sanchez, A., Moore, K., Tian, Z., Zhen, X., Graves, Y. J., Gautier, Q., Mell, L., Zhou, L. et al. (2013). Automatic treatment plan re-optimization for adaptive radiotherapy guided with the initial plan DVHs, *Physics in Medicine and Biology* **58**(24): 8725–8738.

Mahnam, M., Gendreau, M., Lahrichi, N. and Rousseau, L.-M. (2017). Simultaneous delivery time and aperture shape optimization for the volumetric-modulated arc therapy (VMAT) treatment planning problem, *Physics in Medicine and Biology* **62**(14): 5589–5611.

Men, C., Romeijn, H. E., Jia, X. and Jiang, S. B. (2010). Ultrafast treatment plan optimization for volumetric modulated arc therapy (VMAT), *Medical Physics* **37**(11): 5787–5791.

Men, C., Romeijn, H. E., Tas, Z. C. and Dempsey, J. F. (2007). An exact approach to direct aperture optimization in IMRT treatment planning, *Physics in Medicine and Biology* **52**(24): 7333–7352.

Nguyen, D., Lyu, Q., Ruan, D., O'Connor, D., Low, D. A. and Sheng, K. (2016). A comprehensive formulation for volumetric modulated arc therapy planning, *Medical Physics* **43**(7): 4263–4272.

Otto, K. (2008). Volumetric modulated arc therapy: IMRT in a single gantry arc, *Medical Physics* **35**(1): 310–317.

Papp, D. and Unkelbach, J. (2014). Direct leaf trajectory optimization for volumetric modulated arc therapy planning with sliding window delivery, *Medical Physics* **41**(1): 011701.

Peng, F., Jia, X., Gu, X., Epelman, M. A., Romeijn, H. E. and Jiang, S. B. (2012). A new column-generation-based algorithm for VMAT treatment plan optimization, *Physics in Medicine and Biology* **57**(14): 4569–4588.

Peng, F., Jiang, S. B., Romeijn, H. E. and Epelman, M. A. (2015). VMATc: VMAT with constant gantry speed and dose rate, *Physics in Medicine and Biology* **60**(7): 2955–2979.

Preciado-Walters, F., Rardin, R., Langer, M. and Thai, V. (2004). A coupled column generation, mixed integer approach to optimal planning of intensity modulated radiation therapy for cancer, *Mathematical Programming* **101**(2): 319–338.

Renaud, M.-A., Serban, M. and Seuntjens, J. (2017). On mixed electron-photon radiation therapy optimisation using the column generation approach, *Medical Physics* **44**: 4287–4298.

Romeijn, H. E., Ahuja, R. K., Dempsey, J. F. and Kumar, A. (2005). A column generation approach to radiation therapy treatment planning using aperture modulation, *SIAM Journal on Optimization* **15**(3): 838–862.

Romeijn, H. E., Ahuja, R. K., Dempsey, J. F., Kumar, A. and Li, J. G. (2003). A novel linear programming approach to fluence map optimization for intensity modulated radiation therapy treatment planning, *Physics in Medicine and Biology* **48**(21): 3521–3542.

Salari, E., Wala, J. and Craft, D. (2012). Exploring trade-offs between VMAT dose quality and delivery efficiency using a network optimization approach, *Physics in Medicine and Biology* **57**(17): 5587–5600.

Tuncel, A. T., Preciado, F., Rardin, R. L., Langer, M. and Richard, J.-P. P. (2012). Strong valid inequalities for fluence map optimization problem under dose-volume restrictions, *Annals of*

Operations Research **196**(1): 819–840.

Unkelbach, J., Bortfeld, T., Craft, D., Alber, M., Bangert, M., Bokrantz, R., Chen, D., Li, R., Xing, L., Men, C. et al. (2015). Optimization approaches to volumetric modulated arc therapy planning, *Medical Physics* **42**(3): 1367–1377.

Voet, P. W., Dirkx, M. L., Breedveld, S., Fransen, D., Levendag, P. C. and Heijmen, B. J. (2013). Toward fully automated multicriterial plan generation: A prospective clinical study, *International Journal of Radiation Oncology Biology Physics* **85**(3): 866–872.

Wu, Q. and Mohan, R. (2000). Algorithms and functionality of an intensity modulated radiotherapy optimization system, *Medical physics* **27**(4): 701–711.

Zarepisheh, M., Long, T., Li, N., Tian, Z., Romeijn, H. E., Jia, X. and Jiang, S. B. (2014). A DVH-guided IMRT optimization algorithm for automatic treatment planning and adaptive radiotherapy replanning, *Medical Physics* **41**(6): 061711.